Soft-x-ray Cherenkov radiation generated by a charged particle moving near a finite-size screen

M. Shevelev,[1,*] A. Konkov,[2,†] and A. Aryshev[1]
[1]*KEK: High Energy Accelerator Research Organization, 1-1 Oho, Tsukuba, Ibaraki 305-0801, Japan*
[2]*Tomsk Polytechnic University, Institute of Physics and Technology, Lenin Avenue 30, Tomsk 634050, Russian Federation*
(Received 19 August 2015; published 23 November 2015)

This paper demonstrates the application of a polarization current approach to estimate the yield of soft x-ray Cherenkov radiation when a charged particle travels in the vicinity of a finite-size screen. To account for resonant anomalous dispersion of the complex permittivity, we apply the formalism for the atomic scattering factor. We derived the simple analytical expression for the radiation field, which allows us to determine all properties for a wide energy range of emitted radiation of a charged particle. The influence of screen sizes on Cherenkov radiation characteristics is determined by macroscopic and microscopic approaches.

DOI: 10.1103/PhysRevA.92.053851 PACS number(s): 41.60.Bq, 78.70.Dm, 41.60.Dk

I. INTRODUCTION

The significant progress in x-ray microscopy is closely related to the investigation and development of new reflective and diffractive optics [1–3], detectors, imaging methodology [4–7], and new radiation sources. Soft x rays emitting in the water window spectral range, which consists of x rays between the K-shell absorption edges of carbon at 284 eV and oxygen at 543 eV, are ideally suited for imaging live biological samples [4]. The high contrast obtained in this spectral range is due to very strong absorption of carbon in organic specimens, while water is almost transparent [8]. Today there are several different types of radiation sources for the spectral range under consideration. These radiation source facilities differ from each other by physics of emitted radiation, photon flux, and design complexity. Synchrotrons and free-electron lasers are the most powerful sources of soft x-ray radiation and are widely used due to their obvious advantages. However, their dependence on large-scale electron accelerator facilities means that only a few of such sources exist worldwide. There are promising alternative sources such as high-harmonic generated femtosecond laser pulses [9,10] and laser plasma [11,12], but usually do not meet the requirements for photon monochromaticity. Another disadvantage of laser plasma sources is the production of target debris associated with laser ablation. Thereby, the development of new and alternative methods for generating soft x rays will be of great practical significance in the near future. The most promising candidate in the quest for a new monochromatic and high-brightness source of ultraviolet and soft x ray is Cherenkov radiation (ChR) that is generated by electron bunches from a compact accelerator.

As is generally known, ChR occurs when the velocity of a fast charge traveling in a homogeneous medium exceeds the phase velocity of the photons [13–15]. This condition holds for most mediums from the visible to the ultraviolet range. In the 1970s, Piestrup *et al.* [16,17] pursued the development of a radiation source based on the Cherenkov effect for the far and vacuum ultraviolet bands and demonstrated that the radiation power per unit wavelength for ChR is two to three orders of magnitude greater than for synchrotron radiation in the visible and ultraviolet bands. The first experimental demonstration was conducted at the Stanford's High Energy Physics Laboratory in 1973 using a 330-MeV electron beam that traveled in air before striking the quartz or sapphire targets.

According to the classical theory reported previously [18], Cherenkov x rays can also be emitted in the very narrow spectral ranges of resonant anomalous dispersion at the atomic absorption edges such as the K, L, and M edges. This phenomenon was experimentally confirmed by Bazylev and coauthors [19] for carbon at frequencies close to the K edge using 1.2-GeV electrons. In 1990, x-ray ChR was investigated for condition where the 75-MeV electrons were incident on thin foils with small grazing angles of incidence. The experimental tests demonstrated that for grazing angles of incidence the intensity of Cherenkov emission could be more than ten times greater than for normal incidence [20]. The experimental investigations stimulated further theory development of x-ray ChR emitted by ultrarelativistic electrons in the case of very small angles of incidence on thin foils [21–23].

The latest experimental studies performed by Knulst [24] and the theoretical estimates obtained by Kaplan and Shkolnikov [25] in the first decade of this century are of great interest for x-ray microscopy applications. They saw the need to develop a soft x-ray source based on the Cherenkov effect using a compact electron accelerator. To realize this goal, a series of experimental investigations was carried out to show that x-ray brightness, which can be achieved by passing a 5–10-MeV electron beam through a thin foil, is sufficient for practical x-ray microscopy in the water window spectral range [26,27]. It should be mentioned that the authors of the experiments measured the x-ray approximately at the Cherenkov angles and demonstrated that there was reasonable agreement with the model based on the classical theory of transition radiation (TR) [28,29].

From our point of view the main peculiarity of x-ray radiation generated by a low-energy electron beam is the strong interference phenomenon between ChR and TR. This interference is understandable, since both radiation mechanisms may be described as a secondary electromagnetic field produced by polarization currents that emerge from the interaction of an electromagnetic field of a charge with atomic electrons of the medium [30,31]. Zrevol and Ružička were the first to

*Corresponding author: mishe@post.kek.jp
†Corresponding author: ekwinus@tpu.ru

conduct theoretical investigations of this interference effect in the visible wavelength range [32]. They showed that the emitted radiation possessed both TR and ChR properties, i.e., that it is a hybrid radiation. However, despite the critical interest, the theoretical investigations ignored the effect in soft x-ray range under consideration.

To avoid hybrid radiation and investigate only the properties of ChR, the Cherenkov effect may be induced by a constant-velocity charge in rectilinear motion in vacuum in close vicinity to a target [33–37]. The first theoretical work on x-ray diffraction radiation (DR) under the condition for the Cherenkov effect, i.e., the simultaneous emission of ChR and DR when a high-energy charge travels near an absorbing screen, has been reported in [38]. Later, this phenomenon in monograph [39] was studied in greater detail. Unfortunately, the theoretical approach developed in mentioned papers cannot be employed for a low-energy relativistic charge. Therefore, a theoretical investigation of the simultaneous emission of ChR and DR generated by a low-energy relativistic charge is desirable to acquire a better understanding of the radiation's nature. New knowledge on ChR will enable the outlining of the requirements for future experiments to increase the yield of Cherenkov x-rays when an electron beam passes through a target [40]. In this paper, we describe the process of x-ray ChR using the more universal theory [31], wherein the origin of the radiation field is a polarization current induced in the bulk of a medium by the Coulomb field of the initial particle. We discuss radiation properties including the polarization states and dependence of ChR intensity on finite screen sizes and charge energy.

The paper is divided into four sections. In Sec. II we present in detail the theoretical study of Cherenkov x rays and diffraction emission for a charged particle traveling parallel to a finite-size screen using a polarization current approach (PCA). We then discuss all limitations of the approach concerning the assigned task and compare the derived result with a well-known solution [38]. The consideration and discussion of the calculation results are given in Sec. III. Our conclusions and final comments are summarized in Sec. IV.

II. X-RAY CHERENKOV EMISSION AS A RADIATION OF POLARIZATION CURRENTS

A. Polarization current approach

As was mentioned in Introduction, ChR and DR can be considered as radiation generated by polarization currents induced in a medium by the electromagnetic field of a uniformly moving charge. Hence, emitted radiation can be described by the use of PCA as the polarization radiation (PR). The approach was created by Ryazanov and Tilinin [41], who applied it to estimate the TR characteristics from the perfectly conducting focusing targets. Their assumption was to use a current induced on the target surface of a charge particle as the radiation source. However, the clear physical basis of PR, as well as the term itself, was coined and provided by Amusia (refer to [42] and the references therein). Potylitsyn and Karlovets performed further development of the approach [30]. They summarized Ryasanov's approach on the dielectric structure and showed the possibility of the simultaneous generation of DR and ChR when a charge travels near a screen of finite conductivity and finite dimensions. Karlovets used PCA to successfully describe the properties of resonant DR, also known as Smith-Purcell radiation [31]. Subsequent research enabled the generalization of the approach for the case of a charged particle in oblique motion near dielectric targets of finite dimensions [43,44]. The theoretical predictions obtained for the case of oblique motion were subjected to experimental tests [45,46] and displayed good agreement between theory and experiment in the millimeter-wave range. We should also mention the papers [47,48] in which the authors used PCA for the semiclassical description of the TR characteristics from vortex electrons. Below, we consider the fundamentals of PCA.

According to PCA, the PR field emitted by the medium's atoms polarized by the external field $\mathbf{E}^0$ of a passing particle with energy $\gamma = E/mc^2 = 1/\sqrt{1-\beta^2}$ moving rectilinearly and with constant velocity $\mathbf{v} = \boldsymbol{\beta} c$ in a substance (or in its vicinity) can be presented as a solution to the "vacuum" set of macroscopic Maxwell's equations. Here, c is the speed of light and m is the mass of the particle. For a nonmagnetic medium, the density of the polarization currents in the right-hand side of the equation can be written as

$$\mathbf{j}_{\mathrm{pol}} = \sigma(\omega)[\mathbf{E}^0 + \mathbf{E}^{\mathrm{pol}}(\mathbf{j}_{\mathrm{pol}})], \tag{1}$$

where $\mathbf{E}^0 \equiv \mathbf{E}^0(\mathbf{r},\omega)$ and $\mathbf{E}^{\mathrm{pol}} \equiv \mathbf{E}^{\mathrm{pol}}(\mathbf{r},\omega)$ are the respective Fourier images of the particle field in vacuum and the field generated by the currents induced in a medium. The medium's conductivity $\sigma(\omega)$ is related to the dielectric permittivity $\varepsilon(\omega)$ as

$$\sigma(\omega) = \frac{i\omega}{4\pi}[1 - \varepsilon(\omega)], \tag{2}$$

where $\omega = 2\pi c/\lambda$ is the radiation frequency and λ is the emitted radiation wavelength. Solving Maxwell's equations in a wave zone for a target of finite volume V_T, one can derive an expression for the PR magnetic field emitted by the medium's atoms excited by the passing particle in the form below:

$$\mathbf{H}^{\mathrm{pol}}(\mathbf{r},\omega) = \mathrm{curl}\frac{1}{c}\int_{V_T} \sigma(\omega)\mathbf{E}^0(\mathbf{r}',\omega) \times \frac{\exp\left[i\frac{\omega}{c}\sqrt{\varepsilon(\omega)}|\mathbf{r}'-\mathbf{r}|\right]}{|\mathbf{r}'-\mathbf{r}|} d^3r'. \tag{3}$$

In this approach we assume that the energy loss by the particle is negligibly small in comparison to the total energy. Here Eq. (3) is an exact solution of Maxwell's equations, which allows us to avoid solving a differential Eq. (1). When we account for the second term in Eq. (1), the wave number ω/c in vacuum is simply replaced with $\sqrt{\varepsilon(\omega)}\omega/c$. Such a replacement represents a "renormalization" of the particle field inside a medium caused by the field from the polarization currents [31]. Despite its simple form, Eq. (3) describes all types of PR generated in a target of an arbitrary shape.

B. Radiation field in a medium

We consider one of the basic radiation problems: emissions of a charged particle moving near a finite rectangular

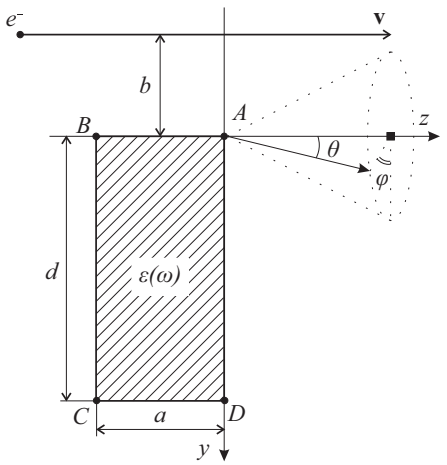

FIG. 1. A schematic view of the radiation geometry for a charged particle moving in the vicinity of a finite-size screen.

conductivity screen (see Fig. 1). For the presented geometry two types of PR arise: DR and ChR. Due to the fact that the polarization currents are induced in a finite volume determined by the screen dimensions, the solution of Eq. (3) can be found in the form

$$\mathbf{H}^{\rm pol}(\mathbf{r},\omega) = \frac{2\pi i}{c}\frac{e^{ikr}}{r}\mathbf{k}\int_{-a}^{0}dz'\int_{0}^{d}\sigma(\omega)\mathbf{E}^{0}(k_x,y',z',\omega) \times e^{-i(y'k_y+z'k_z)}dy', \tag{4}$$

where $\mathbf{k} = \omega\sqrt{\varepsilon(\omega)}\mathbf{e}/c$ is the wave vector and $\mathbf{e} = \mathbf{r}/r$ is the unit vector along the photon emission. Accounting for Snell's law of refraction, the unit vector is

$$\mathbf{e} = \begin{pmatrix}\sin\theta_m\sin\phi\\ \sin\theta_m\cos\phi\\ \cos\theta_m\end{pmatrix} = \frac{1}{\sqrt{\varepsilon}}\begin{pmatrix}\sin\theta\sin\phi\\ \sin\theta\cos\phi\\ \sqrt{\varepsilon-\sin^2\theta}\end{pmatrix}, \tag{5}$$

where θ_m and θ are the respective polar angles for a medium and in vacuum and ϕ is the azimuthal angle. For simplicity we apply $\varepsilon(\omega) = \varepsilon$.

In Eq. (4), the range of integration is reduced only to the volume of the medium (target). We assume the screen to be infinity in the x direction, which is perpendicular to the plane of Fig. 1. This statement is principally true when the screen dimension in the x direction becomes much larger than the effective size of a charged-particle field $\sim\gamma\lambda$. To find the solution for Eq. (4), we need the Fourier component of the charged-particle field. Since we know the complete Fourier image of the field in the equation [49]

$$\mathbf{E}^{0}(\mathbf{k},\omega) = \frac{4\pi i}{\omega}\frac{\mathbf{j}^{0}(\mathbf{k},\omega)\omega^2/c^2 - \mathbf{k}[\mathbf{k}\cdot\mathbf{j}^{0}(\mathbf{k},\omega)]}{\mathbf{k}^2-\omega^2/c^2}, \tag{6}$$

we can derive the expression for the Fourier component as

$$\mathbf{E}^{0}(k_x,y',z',\omega) = \int_{-\infty}^{\infty}dk_y\int_{-\infty}^{\infty}\mathbf{E}^{0}(\mathbf{k},\omega)e^{i(y'k_y+z'k_z)}dk_z. \tag{7}$$

In Eq. (6) the Fourier image of a particle current's density is

$$\mathbf{j}^{0}(\mathbf{k},\omega) = \frac{e\mathbf{v}}{(2\pi)^3}\delta(\mathbf{k}\cdot\mathbf{v}-\omega)\exp[ik_y b], \tag{8}$$

where e is the particle charge, $\mathbf{v} = (0,0,v)$ is the particle velocity vector, $\delta(\mathbf{k}\cdot\mathbf{v}-\omega)$ is the Dirac δ function, and b is the distance from the particle trajectory to the edge of the target (impact factor).

The Fourier component of a uniformly moving charge field entering the current density $\mathbf{j}^{0}(\mathbf{k},\omega)$ is readily expressed by the equation

$$\mathbf{E}^{0}(k_x,y,z,\omega) = -\frac{ie}{2\pi vK}\exp\left[i\frac{\omega}{v}z\right](\gamma\beta e_x\sqrt{\varepsilon},iK,\gamma^{-1}) \times\exp\left[-\frac{\omega}{v\gamma}(y+b)K\right], \tag{9}$$

where $K = \sqrt{1+(\gamma\beta e_x)^2\varepsilon}$.

Substituting Eqs. (2) and (9) in Eq. (4) and integrating over the target volume, we can obtain an expression for the PR field strength,

$$\mathbf{H}^{\rm pol}(\mathbf{r},\omega) = \frac{e\beta}{4\pi c}\frac{(\varepsilon-1)\sqrt{\varepsilon}}{K}\frac{\exp\left[i\frac{\omega}{c}\sqrt{\varepsilon}r\right]}{r}\mathbf{F} \times\frac{1-\exp\left[-ia\frac{\omega}{\beta c}(1-\beta\sqrt{\varepsilon}e_z)\right]}{1-\beta\sqrt{\varepsilon}e_z} \times\exp\left[-b\frac{\omega}{\beta c}\gamma^{-1}K\right] \times\frac{\exp\left[-d\frac{\omega}{\beta c}(\gamma^{-1}K+i\beta\sqrt{\varepsilon}e_y)\right]-1}{\gamma^{-1}K+i\beta\sqrt{\varepsilon}e_y}, \tag{10}$$

where we have used the following designations:

$$\mathbf{F} = \begin{pmatrix}\gamma^{-1}e_y - iKe_z\\ (\gamma\beta\sqrt{\varepsilon}e_z-\gamma^{-1})e_x\\ (iK-\gamma\beta\sqrt{\varepsilon}e_y)e_x\end{pmatrix}. \tag{11}$$

C. Optical properties of medium in x-ray range near the absorption edges

In the x-ray frequency range, permittivity is usually calculated with what is also known as the plasma formula [50]:

$$\varepsilon(\omega) = 1-\left(\frac{\hbar\omega_p}{\hbar\omega}\right)^2. \tag{12}$$

It is also assumed that all atomic electrons respond to the x-ray radiation as if they are free $\hbar\omega \gg \hbar\omega_p$, i.e., as if the emitted photon energy $\hbar\omega$ is larger than the plasmon energy in the target material,

$$\hbar\omega_p = \sqrt{4\pi n_e r_0(\hbar c)^2} = \sqrt{4\pi\frac{Z}{A}N_0\rho r_0(\hbar c)^2}, \tag{13}$$

where n_e is the concentration of free electron in matter, $r_0 = e^2/(m_0c^2)$ is the classical electron radius, Z and A are the atomic number and the atomic mass number, respectively, N_0 is the Avogadro constant, and ρ is the matter density.

However, in the frequency range when $\hbar\omega > 30$ eV, the free-electron approximation is invalid because the energy of the emitted radiation is comparable to the energy of electrons at the atomic outer shell. In the case under consideration, the propagation of an electromagnetic wave in a medium is accompanied by radiation scattering from all atomic dipoles. These dipoles occur as a result of the distortion of the outer electron shells of the atoms under radiation influence [24]. The emission of the electromagnetic waves with energy $\hbar\omega_s$ (where ω_s is the natural frequency of atomic dipole) is caused by the tendency of the formed dipoles to return to the initial condition. Dipole radiation, in turn, interferes with the scattering radiation of the electromagnetic waves. When the frequency of the incident wave is the same as the frequency of the natural dipole oscillation ($\omega = \omega_s$), the resonant change of the dielectric properties of the medium (anomalous dispersion) and a sharp rise in photon yield occur [51]. The above-mentioned resonance condition is satisfied only at frequencies ω_q that correspond to the atomic absorption edges.

Therefore, it is necessary to use a more general model for dielectric permittivity instead of plasma formula (12) to describe the optical properties of matter in the frequency range being considered. The plasma formula is invalid at the absorption edges due to anomalous dispersion. Accounting for the anomalous dispersion, we calculate the dielectric permittivity in terms of the complex atomic scattering factor $f(\omega)$ [8,52],

$$f(\omega) = f_1(\omega) \pm i f_2(\omega), \tag{14}$$

where factors $f_1(\omega)$, $f_2(\omega)$ are real and can be derived from the Kramers-Kronig relations

$$f_1(\omega) = Z + \frac{1}{2\pi^2 r_0 c} \sum_q \int_{\omega_q}^{\infty} \frac{\omega_s^2\left(\omega^2 - \omega_s^2\right) Z_q \mu_q(\omega_s) d\omega_s}{\left(\omega^2 - \omega_s^2\right)^2 + \Gamma_q^2 \omega^4},$$
$$f_2(\omega) = \frac{1}{2\pi^2 r_0 c} \sum_q \int_{\omega_q}^{\infty} \frac{\omega_s^2 \Gamma_q \omega^2 Z_q \mu_q(\omega_s) d\omega_s}{\left(\omega^2 - \omega_s^2\right)^2 + \Gamma_q^2 \omega^4}, \tag{15}$$

where Z_q is the number of q-shell electrons, $\mu_q(\omega_s)$ is the cross section for photoionization of q-shell electrons by a photon with frequency ω_s, and Γ_q is the damping factor that is usually determined by experimentation.

Therefore, the interaction of x rays with the medium can be described by the model of dielectric permittivity developed by Henke [8]:

$$\varepsilon(\omega) = \left[1 - \frac{1}{2Z}\left(\frac{\hbar\omega_p}{\hbar\omega}\right)^2 f(\omega)\right]^2. \tag{16}$$

For frequencies higher than the eigenfrequencies of atomic electrons ($\hbar\omega \gg \hbar\omega_p$), Eq. (16) becomes the well-known plasma formula, since the value of the integral term of Eq. (15) is small in comparison with the first term of factor $f_1(\omega)$. We should also note that the contribution of higher-order terms from Eq. (16) will be negligible for the high-frequency range.

It is also noteworthy that an ambiguity in the sign between the coefficients $f_1(\omega)$ and $f_2(\omega)$ that actually determine the real and imaginary parts of the dielectric permittivity is present in Eq. (14). The choice of sign allows us to describe both passive (absorption of the radiation) and active mediums (stimulation of the radiation). At the same time, the medium properties will directly depend on the sign in front of the phase term (spread factor) of Maxwell's equation solution for a plane electromagnetic wave [53]. To verify the last statement, let us consider propagation of a plane electromagnetic wave,

$$\mathbf{E}(\mathbf{r},t) = (E_0 \exp[\pm i\omega t \pm \kappa z],0,0),$$
$$\mathbf{H}(\mathbf{r},t) = (0,H_0 \exp[\pm i\omega t \pm \kappa z],0), \tag{17}$$

in the $\pm z$ directions. The plane-wave phase $\exp[\pm i\omega t \pm \kappa z]$ includes two independent signs. The sign before $i\omega$ is chosen according to the accepted convention. However, an ambiguity in the sign before κz persists because Maxwell's equations allow both treatments. Note that the $+i\omega$ sign convention is commonly used by American and European physical societies (refer to the Feynman lectures on physics [54]), while in Russian the $-i\omega$ sign convention is usually accepted (refer to the course of theoretical physics written by Landau and Lifshitz [55]). To prove this statement, we can substitute solution (17) into Maxwell's equations, which describe Faraday's law and Ampere-Maxwell's law,

$$\nabla \times \mathbf{E}(\mathbf{r},t) = -\mu \frac{\partial \mathbf{H}(\mathbf{r},t)}{\partial t},$$
$$\nabla \times \mathbf{H}(\mathbf{r},t) = \sigma\, \mathbf{E}(\mathbf{r},t) + \varepsilon \frac{\partial \mathbf{E}(\mathbf{r},t)}{\partial t}, \tag{18}$$

where μ is the magnetic permeability. Solving the system (18) for κ, we obtain

$$\kappa^2 = \pm i\omega\mu(\sigma \pm i\omega\varepsilon). \tag{19}$$

The next step is the choice of the sign before $i\omega$ according to the accepted convention, for instance, $+i\omega$. Therefore, transforming Eq. (19) we have two independent solutions:

$$\kappa = \pm i\omega\sqrt{\varepsilon\mu}\sqrt{1 - i\frac{\sigma}{\omega\varepsilon}}$$
$$= \pm i\omega\sqrt{\varepsilon\mu}\sqrt{1 + \frac{\sigma^2}{\omega^2\varepsilon^2}} \exp\left[-\frac{i}{2}\arctan\left(\frac{\sigma}{\omega\varepsilon}\right)\right]. \tag{20}$$

Note that the phase term in Eq. (20) has the same sign as in the accepted convention. Thus, the electromagnetic wave phase, which propagates in the z direction, decreases at any time t. In the case being considered we should use the negative sign in Eq. (20). A consequence of the choice of sign is the decrease proportional to $\kappa = \omega\sqrt{\varepsilon\mu}$ of an electromagnetic wave phase. In this way, the real part of the spread factor has the sign $\propto -i\,(-i)\arctan[\sigma/(\omega\varepsilon)]$, the sign being negative for positive conductivity (passive medium). The obtained result is correct because the amplitude of an electromagnetic wave, which propagates in the $+z$ direction in a passive medium, drops with increasing z. Similarly, when we use the positive sign in Eq. (20), the electromagnetic wave phase rises with increasing z. Hence, an electromagnetic wave spreads in the negative z direction. In this case, the real part of spread factor has a positive sign for an absorbing medium, with an electromagnetic wave amplitude that increases with increasing z. We can derive similar results using the other convention ($-i\omega$). However, incorrect choice of the sign

between the parts of complex dielectric permittivity and/or magnetic permeability leads to an incorrect sign before the real part of the spread factor, which will result in an active medium being incorrectly considered to be passive. In other words, for correctly describing the matter's dielectric properties, it is necessary to follow the guidance from the principle of causality [56]. According to this principle, the intensity of an electromagnetic wave spreading from the interface between vacuum and matter must decrease for matter in thermodynamic equilibrium.

D. Radiation field in vacuum

To find the radiation field in vacuum we should use the reciprocity theorem [55] according to the application of this approach,

$$|\mathbf{E}^{\mathrm{pol(vacuum)}}| = \left|\frac{1}{\sqrt{\varepsilon}}\mathbf{E}^{\mathrm{pol(medium)}}\right| = \frac{1}{|\varepsilon|^2}|\mathbf{H}^{\mathrm{pol(medium)}}|, \tag{21}$$

where $\mathbf{E}^{\mathrm{pol(vacuum)}}$ is the radiation field in vacuum generated by the dipole in a medium and $\mathbf{E}^{\mathrm{pol(medium)}}$ is the radiation field in the medium generated by the dipole placed in vacuum at a large distance from the interface. In Eq. (21) we use the relationship between electric and magnetic fields. The spectral-angular distribution of PR in vacuum can be defined as

$$\begin{aligned}\frac{d^2W}{d\omega d\Omega} &= cr^2|\mathbf{E}^{\mathrm{pol(vacuum)}}|^2 \\ &= \frac{cr^2}{|\varepsilon|^2}[|f_H|^2|H_\perp^{\mathrm{pol}}|^2 + |\sqrt{\varepsilon}f_E|^2|H_{||}^{\mathrm{pol}}|^2] \\ &= \frac{cr^2}{|\varepsilon|^2}\left[|f_H|^2\left|H_x^{\mathrm{pol}}\cos\phi - H_y^{\mathrm{pol}}\sin\phi\right|^2 + |\sqrt{\varepsilon}f_E|^2\right. \\ &\quad \left.\times\left|\sqrt{\left(H_z^{\mathrm{pol}}\right)^2 + \left(H_x^{\mathrm{pol}}\sin\phi + H_y^{\mathrm{pol}}\cos\phi\right)^2}\right|^2\right].\end{aligned} \tag{22}$$

The Fresnel equations for an infinite boundary are given by

$$\begin{aligned} f_H &= \frac{2\varepsilon\cos\theta}{\varepsilon\cos\theta + \sqrt{\varepsilon - \sin^2\theta}}, \\ f_E &= \frac{2\cos\theta}{\cos\theta + \sqrt{\varepsilon - \sin^2\theta}}. \end{aligned} \tag{23}$$

In x-ray range, the Fresnel equations are equal to unity for many different materials, as shown in Fig. 2. Clearly, the PR spectral-angular distributions in vacuum and in the medium are the same. The eikonal approximation is valid in the high-frequency range for most materials and the relative error is always a few percent or less (e.g., for photon energies near the absorption L edge of carbon and aluminum the relative errors are 2% and 4%, respectively). Therefore, Eq. (22) can be represented in simplified form as

$$\frac{d^2W}{d\omega d\Omega} = cr^2|\mathbf{E}^{\mathrm{pol}}(\mathbf{r},\omega)|^2, \tag{24}$$

where $\mathbf{E}^{\mathrm{pol}}(\mathbf{r},\omega) = -\mathbf{e}\times\mathbf{H}^{\mathrm{pol}}(\mathbf{r},\omega)/\sqrt{\varepsilon}$.

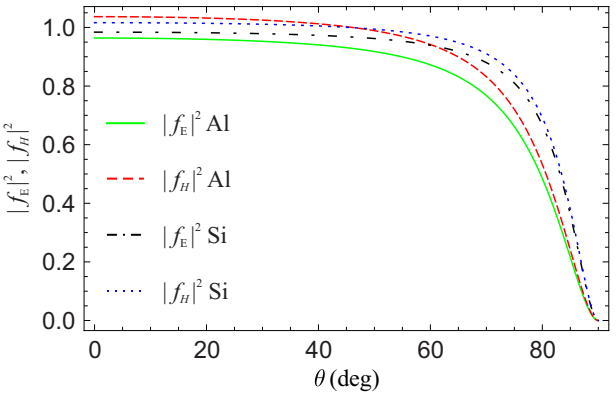

FIG. 2. (Color online) Fresnel equations as a function of observation angle θ. The solid green and dashed red curves correspond, respectively, to Fresnel equations for electric and magnetic components of an incident wave impinging on an aluminum-vacuum boundary. The x-ray energy near the L-edge absorption of aluminum is 72.6 eV. The dot-dashed black and the dotted blue curves correspond, respectively, to Fresnel equations for electric and magnetic components of an incident wave impinging on a silicon-vacuum boundary, respectively. The x-ray energy near the L-edge absorption of silicon is 99.8 eV.

The final expression for the spectral-angular distribution of PR in the forward direction (the positive direction of the z axis) for a charged particle not directly intersecting a screen is defined as

$$\begin{aligned}\frac{d^2W}{d\omega d\Omega} &= \frac{e^2\beta^2}{16\pi^2 c}\left|\frac{(\varepsilon-1)}{K}\mathbf{F}\right|^2\left|\frac{\exp\left[-d\frac{\omega}{\beta c}\Sigma\right]-1}{\Sigma}\right|^2 \\ &\quad\times\left|\frac{1-\exp\left[-ia\frac{\omega}{\beta c}P\right]}{P}\right|^2\exp\left[-2b\frac{\omega}{\gamma\beta c}\,\mathrm{Re}\,K\right],\end{aligned} \tag{25}$$

where we used the following notations and relationship for the polar angles $\theta_m \equiv \theta$:

$$\begin{aligned} P &= 1 - \beta\sqrt{\varepsilon}\cos\theta, \\ \Sigma &= \gamma^{-1}K + i\beta\sqrt{\varepsilon}\sin\theta\cos\phi, \\ K &= \sqrt{1 + (\gamma\beta\sin\theta\sin\phi)^2\varepsilon}. \end{aligned}$$

Equation (25) describes the spectral-angular density of PR and accounts for both DR and ChR. Cherenkov emission corresponds to the pole in the denominator:

$$|1 - \beta\sqrt{\varepsilon}\cos\theta| \to 0.$$

This expression leads to the well-known Vavilov-Cherenkov condition.

E. Stokes parameters for PR

The use of the Stokes parameters is the most effective way to describe the polarization properties of PR. The Stokes parameters are a set of values that provide full information on the polarization state and intensity of electromagnetic

radiation [57–60],

$$\xi_1 = \frac{E_1^* E_1 - E_2 E_2^*}{E_1^* E_1 + E_2 E_2^*},$$
$$\xi_2 = i\frac{E_1^* E_2 - E_1 E_2^*}{E_1^* E_1 + E_2 E_2^*}, \tag{26}$$
$$\xi_3 = \frac{E_1^* E_2 + E_1 E_2^*}{E_1^* E_1 + E_2 E_2^*},$$

where E_1 and E_2 are the electric-field components orthogonal to the direction of radiation propagation. The asterisk represents the complex conjugate.

The first Stokes parameter ξ_1 describes the amount of linear horizontal or vertical polarization along the axis defined by the unit vector $\mathbf{e}_1$, the second parameter ξ_2 helps to determine the amount of right or left circular polarization, and the third parameter ξ_3 corresponds to the amount of linear $\pm 45^\circ$ polarization along the mentioned axis.

To determine the electric-field components E_1 and E_2 in Eqs. (26), the following equations for system of polarization unit vectors can be applied,

$$\mathbf{e}_1 = \frac{[\mathbf{e}\times\mathbf{n}]}{|[\mathbf{e}\times\mathbf{n}]|}, \quad \mathbf{e}_2 = [\mathbf{e}\times\mathbf{e}_1], \tag{27}$$

where $\mathbf{n}$ is the unit vector along the target surface normal.

Thus, the vector components of the PR electric-field strength may be expressed as

$$E_1 = [\mathbf{e}_1 \cdot \mathbf{E}^{\mathrm{pol}}(\mathbf{r},\omega)],$$
$$E_2 = [\mathbf{e}_2 \cdot \mathbf{E}^{\mathrm{pol}}(\mathbf{r},\omega)], \tag{28}$$
$$E_3 = [\mathbf{k} \cdot \mathbf{E}^{\mathrm{pol}}(\mathbf{r},\omega)] = 0.$$

The PR electric-field strength $\mathbf{E}^{\mathrm{pol}}(\mathbf{r},\omega)$ is associated with the magnetic-field strength $\mathbf{H}^{\mathrm{pol}}(\mathbf{r},\omega)$ by the well-known relationship [61]

$$\mathbf{E}^{\mathrm{pol}}(\mathbf{r},\omega) = -\frac{1}{\sqrt{\varepsilon}}[\mathbf{e}\times\mathbf{H}^{\mathrm{pol}}(\mathbf{r},\omega)],$$
$$\mathbf{H}^{\mathrm{pol}}(\mathbf{r},\omega) = \sqrt{\varepsilon}[\mathbf{e}\times\mathbf{E}^{\mathrm{pol}}(\mathbf{r},\omega)]. \tag{29}$$

To calculate the polarization properties of radiation in a medium using Eqs. (26), it is necessary to obtain the magnetic-field strength $\mathbf{H}^{\mathrm{pol}}(\mathbf{r},\omega)$ from Eq. (10) and then describe the electric-field strength in the form of two orthogonal components using relationships (28) and (29). Note that the obtained result describes the polarization properties of radiation in vacuum, where the eikonal approximation is valid and the influence of reflection and refraction at the target edges can be neglected. Otherwise, refraction and reflection effects must be considered. For this purpose, the obtained components of electric field E_1 and E_2 must be multiplied by the corresponding Fresnel equations f_E and f_H. We must also express the radiation angles in the medium (θ_m,ϕ) in terms of corresponding radiation angles in vacuum (θ,ϕ) using Snell's law and account for the association between the field strengths (21).

For the geometry of radiation where the normal vector to the target surface $\mathbf{n}$ is equal to (0,0,1), the polarization unit vectors can be written as follows:

$$\mathbf{e}_1 = \frac{(e_y, -e_x, 0)}{\sqrt{e_x^2+e_y^2}}, \quad \mathbf{e}_2 = \frac{\left(e_x e_z, e_y e_z, -\left(1-e_z^2\right)\right)}{\sqrt{e_x^2+e_y^2}}. \tag{30}$$

Then, using Eqs. (28) and (29), we obtain the components of the electric strength field:

$$E_1 = -\frac{\mathbf{e}_1 \cdot \mathbf{e}\times\mathbf{H}^{\mathrm{pol(vac)}}(\mathbf{r},\omega)}{\sqrt{\varepsilon}} = C\,\frac{\gamma\beta\sqrt{\varepsilon}\sin^2\theta\cos\phi\sin\phi + iK(\cos^2\theta - \sin^3\theta\sin\phi)}{\sin\theta},$$
$$E_2 = -\frac{\mathbf{e}_2 \cdot \mathbf{e}\times\mathbf{H}^{\mathrm{pol(vac)}}(\mathbf{r},\omega)}{\sqrt{\varepsilon}}$$
$$= -C\,\sin^3\theta[\gamma^{-1}\sin\theta\cos^2\phi(\cos\theta\sin\phi+\sin\theta) - iK\cos\theta\cos\phi(\cos\theta\sin\phi+\sin\theta) - \sin^2\phi(\gamma\beta\sqrt{\varepsilon}\cos\theta - \gamma^{-1})$$
$$-(\gamma\beta\sqrt{\varepsilon}\sin\theta\cos\phi - iK)\sin\theta\cos\phi\sin^2\phi(\cos\theta - \sin\theta\sin\phi)],$$
$$E_3 = -\frac{\mathbf{k}\cdot\mathbf{e}\times\mathbf{H}^{\mathrm{pol(vac)}}(\mathbf{r},\omega)}{\sqrt{\varepsilon}} = 0. \tag{31}$$

Here we introduce a convenient notation for the scalar part of the vector of the magnetic strength field:

$$C = \frac{e\beta}{4\pi c}\frac{(\varepsilon-1)}{K}\frac{\exp\left[i\frac{\omega}{c}\sqrt{\varepsilon}r\right]}{r}\frac{\exp\left[-d\frac{\omega}{\beta c}\Sigma\right]-1}{\Sigma}\exp\left[-b\frac{\omega}{\beta c}\gamma^{-1}K\right]\frac{1-\exp\left[-ia\frac{\omega}{\beta c}P\right]}{P}. \tag{32}$$

Finally, using Eq. (26) we can calculate the Stokes parameters. In this paper the final equations for the Stokes parameters are not shown because they are cumbersome to view. However, Eqs. (31) obtained above show that DR and ChR have an elliptical polarization.

F. Limitations of PCA

All theories have their limitations and PCA is not an exception. Since the developed approach is based on macroscopic Maxwell's equations, it must meet the applicability limits of the macroscopic approach of classical electrodynamics. The applicability range for the macroscopic approach in the radiation theory has been analyzed in detail by Ryazanov [62]. Considering TR as a process of reflection and refraction of the self-field of a charge from the interface between two mediums, Ryazanov has shown that, based on condition for frequency conservation of an electromagnetic field and tangential components of a wave vector to the section plane,

two criteria for the applicability of a macroscopic approach occur:

$$ka_0 \ll 1, \tag{33}$$

$$(\omega - k_x v_x - k_y v_y)\frac{a_0}{v_z} \ll 1. \tag{34}$$

The smallest value of the wave vector $\mathbf{k}$ of the emitted wave in comparison with the inverse interatomic distance a_0^{-1} is the main condition (33). Nevertheless, when condition (34) is violated, the macroscopic approach becomes inapplicable, even if condition (33) is fulfilled. When the speed factor v_z in the direction of a charged-particle motion is small (i.e., for the nonrelativistic energy or for oblique incidence condition when the speed vector of a charged particle is parallel to the target plane), condition (34) is not fulfilled.

The next restriction is a direct consequence of applying Ohm's law in differential form [see Eq. (1)]. Although Ohm's law may be derived from Maxwell's equations, Ohm's law is an empirical law if conditions (33) and (34) are satisfied, rather than a fundamental physical law [63]. For this reason, there may be violations of Ohm's law [64,65] such as for the following: substances that have superconductive properties at law temperature, conductive and dielectric mediums at high temperature, the strong and high-frequency electromagnetic fields. The use of Ohm's law for plasma, gaseous, and inhomogeneous medium is a nontrivial task and requires detailed consideration.

For the case of an external effect on the target (variation of temperature, pressure or application of electromagnetic field), the macroscopic properties of a substance may vary due to different processes, such as a variation in the number of carriers, appearance of inertia effects, breakdowns, and discharges. All the above-mentioned effects cause a disturbance of linear dependence of the polarization current density $\mathbf{j}^{\mathrm{pol}}$ as a function of the intensity of electric field $\mathbf{E} = \mathbf{E}^0 + \mathbf{E}^{\mathrm{pol}}$.

The critical limitation of the developed approach is the use of the Fresnel equations to determine the spectral-angular distribution of PR in vacuum. Since the obtained Fresnel equations were for an ideal and flat surface without any roughness, the obtained results are valid for a medium with sharp boundaries. In practice, the real surfaces of a target have roughness with dimension of t_d. To use PCA for such target surfaces, it is necessary for the roughness of the boundary surface to be much less than the wavelength of emitted radiation [66]:

$$t_d \ll \lambda. \tag{35}$$

Thus, the limits of PCA application are determined by inequalities in (33) and (34), as well as by the scope of Eq. (1).

G. Verification of obtained result

As we mentioned above, the investigation of DR under condition for the Cherenkov effect has been the subject of several works [38,39]. However, the results obtained by the previous works apply to the case of a charge particle at an ultrarelativistic velocity at a high frequency. Hence, for an appropriate comparison with a well-known solution we must use a straightforward expansion method for solving Eq. (25) that contains the small parameters $\gamma^{-1} \ll 1$, $\theta \ll 1$, and express the dielectric permittivity as

$$\varepsilon(\omega) = 1 + \chi'(\omega) + i\chi''(\omega), \tag{36}$$

where $\chi'(\omega) = -\omega_p^2/\omega^2 \ll 1$ and $\chi''(\omega) \ll 1$.

Thus, after expansion and keeping only the dominant first-order terms in Eq. (25) we obtain

$$\begin{aligned} P &= \frac{1}{2}(\gamma^{-2} + \theta^2 - \chi' - i\chi''), \\ \Sigma &= \gamma^{-1}K + i\theta\cos\phi\left(1 + \frac{\chi' + i\chi''}{2}\right), \\ K &= \sqrt{1 + (\gamma\theta\sin\phi)^2\varepsilon}, \\ \mathbf{F} &= \begin{pmatrix} \gamma^{-1}\theta\cos\phi - iK\left(1 - \frac{\theta^2}{2}\right) \\ \left(1 - \frac{\theta^2 + \gamma^{-2} - \chi' - i\chi''}{2}\right)\gamma\theta\sin\phi \\ i\gamma\Sigma\theta\sin\phi \end{pmatrix}. \end{aligned} \tag{37}$$

Substituting Eqs. (36) and (37) in Eq. (25) and then considering the case of the infinite-size screen ($d \to \infty$), we get

$$\begin{aligned} \frac{d^2W}{d\omega d\Omega} = \frac{e^2}{\pi^2 c}\frac{\chi^2}{\gamma^{-2} + \theta^2}\frac{\left|1 - \exp\left[-ia\frac{\omega}{2\beta c}(\gamma^{-2} + \theta^2 - \chi')\right]\exp\left[-a\frac{\omega}{2\beta c}\chi''\right]\right|^2}{(\gamma^{-2} + \theta^2 - \chi')^2 + (\chi'')^2}\frac{1 + 2(\gamma\theta\sin\phi)^2}{1 + (\gamma\theta\sin\phi)^2} \\ \times \exp\left[-2b\frac{\omega}{\gamma\beta c}\sqrt{1 + (\gamma\theta\sin\phi)^2}\right], \end{aligned} \tag{38}$$

where $\chi^2 = |\chi' + i\chi''|^2$.

For ultrarelativistic velocities $\beta = 1$, Eq. (38) obtained above agrees with the solution from previous works [38,39]. Therefore, our result shows that PCA is a more universal approach, which makes it possible to obtain the properties of x-ray ChR for a wide energy range of a charged particle.

III. RESULTS AND DISCUSSION

A. Spectral-angular distribution of forward PR

The properties of x-ray ChR depend strongly on the dielectric permittivity of the target material. To use PCA, the target material must satisfy several criteria. First, it must be a commonly used condensed matter with known

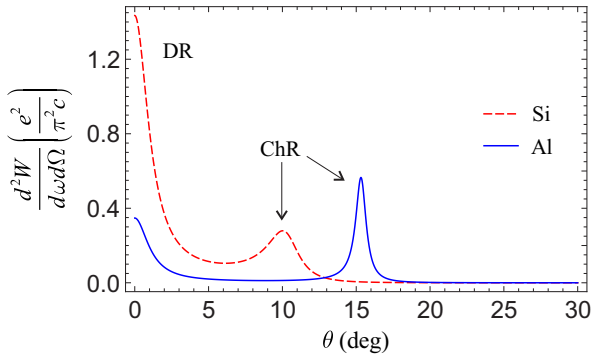

FIG. 3. (Color online) Spectral-angular distribution of PR in θ, emitted by an electron of energy $\gamma = 50$ from various target material. The photon energies: x-ray near absorption L edge of silicon is 99.8 eV (red dashed line), x-ray near absorption L edge of aluminum is 72.6 eV (blue line). Parameters are $a = 0.1$ mm, $d = 10$ mm, $b = 1$ μm, and $\phi = 0$. Notice that distributions have scale factors for better presentation: 10^6 for silicon and 10^3 for aluminum.

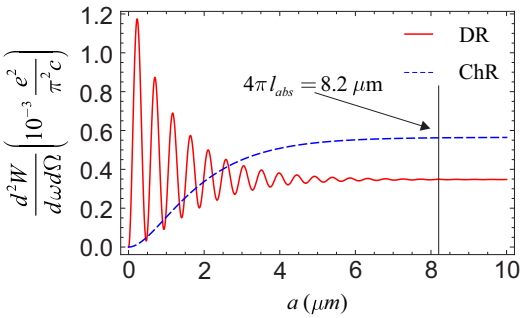

FIG. 4. (Color online) The PR intensity emitted by an electron of energy $\gamma = 50$ at maximum of spectra-angular distribution in θ as a function of longitudinal size a of aluminum foil. The red solid and the blue dashed curves correspond to the forward DR ($\theta = 0$) and ChR ($\theta_c = 15.31^\circ$), respectively. Parameters are $d = 10$ mm, $b = 1$ μm, $\phi = 0$, the energy of x ray near the absorption L edge of aluminum is 72.6 eV.

permittivity near the absorption edge. Second, the angular spread of Cherenkov emission determined by the real part of the complex permittivity should be as large as possible. Thus, the interference phenomenon between ChR and forward DR will not be prominent in spectral-angular distribution and would clearly simplify the explanation of the obtained results.

For silicon and aluminum the spectral-angular distributions of the forward PR obtained by Eq. (25) are shown in Fig. 3 with the following parameter selection: screen dimensions are $a = 0.1$ mm, $d = 10$ mm; impact factor b is equal to 1 μm; and the electron energy is $\gamma = 50$. One can easily see that Cherenkov x rays are emitted in the forward direction at an angle relative to the charge trajectory θ_c given by $\cos\theta_c = c/\mathrm{Re}\sqrt{\varepsilon}v$, whereas the spread of the forward DR occurs along the direction of the charge trajectory. In Table I we list the data for commonly used materials. The spectral-angular distribution of PR for carbon and titanium are not shown in Fig. 3, since the increase in energy of emitted photons leads to a drop in radiation intensity for the considered calculation parameters. For example, the intensities of carbon and silicon differ by 15 orders of magnitude. Using the absolute value of the emitted energy distribution presented in Fig. 3 one can estimate the average number of emitted photons per electron. As is seen from Fig. 3 aluminum foil satisfies the mentioned criteria.

According to the derived results based on Eqs. (26) and (31), DR ($\theta = 0$) and ChR ($\theta_c = 15.31^\circ$) in the plane $\phi = 0$ from the aluminum screen have a linear polarization: $\xi_1^{\mathrm{DR}} = 100\%$, $\xi_1^{\mathrm{ChR}} = 99.85\%$, and $\xi_3^{\mathrm{ChR}} = 0.15\%$.

TABLE I. Table of considered Cherenkov radiators. The energy of emitted photons corresponds to absorption edges of materials (the K edge for C, and L edge for Al, Si, and Ti).

Material	$\hbar\omega$ (eV)	ε	θ_c (deg)
Al	72.6	1.07559–0.00437i	15.31
Si	99.8	1.03275–0.00851i	10.02
C	284	1.00734–0.00276i	4.75
Ti	453.8	1.00698–0.00197i	4.53

B. PR from an absorbing medium with the sharp boundaries

Numerous investigations have been devoted to electromagnetic radiation generated by a charge in an absorbing medium for different frequency ranges [19,30,67–69]. In this section we investigate the effect of absorption by the medium and target's sharp boundaries on the x-ray PR generated by an electron moving near an absorbing screen of finite dimensions. The influence of the screen's finite sizes on the radiation intensity is considered by both macroscopic and microscopic methods in electrodynamics.

Let us consider the dependence of the intensity of emitted photons in the given directions corresponding to the maximum value in a spectral-angular distribution of PR on the longitudinal dimension of screen a (see Fig. 1). Figure 4 shows dependencies that correspond to the different respective observation angles $\theta = 0$ and $\theta_c = 15.31^\circ$ for forward DR and ChR. The selected calculation parameters are as follows: impact factor is $b = 1$ μm, transverse size of screen is $d = 10$ mm, and the electron energy is $\gamma = 50$.

We observe that the dependence of the forward DR is a rapidly oscillating function, which undergoes attenuation with increasing longitudinal screen size, whereas the dependence of ChR rises with increasing longitudinal foil size and then saturates. To describe the features of electromagnetic radiation for a medium with sharp boundaries, we need to address several aspects. The first aspect relates to the radiation coherence length, which is also called the formation length. The second aspect is the influence of the absorption properties of a medium on radiation processes.

Now let us discuss the coherence length of forward DR. To avoid any possible confusions with the term, it may be helpful to remember that from classical formalism in electromagnetic theory the coherence length can be defined as the length of the particle path section such that the fields of radiation produced from all its points arrive at the observation point with almost the same phases and are coherently summed [67]. Potylitsyn

et al. consider the qualitative explanation of coherence length of forward DR using microscopic theory [39]. The condition of the coherence length in a medium can be written in the following form:

$$l_{\mathrm{coh}} \sim \frac{\lambda}{|\beta^{-1} - \mathrm{Re}\sqrt{\varepsilon}|}. \tag{39}$$

After a detailed analysis the authors showed that two atoms of the medium emit coherently if the distance L between them is equal to an integer number of coherence lengths l_{coh}.

For forward DR, the radiation sources are the polarization currents occurring in the surface layers of the interface between two mediums (BC and AD facets in Fig. 1); refer to Ref. [44]. Nevertheless, all estimations of coherent length obtained from microscopic theory could be applied to understand the results obtained by the macroscopic approach. As one can see from Fig. 4, the dependence of the forward DR intensity on the longitudinal screen size is a periodic function with period $l_{\mathrm{coh}} = 469$ nm. The maximums of the oscillating function correspond to when the two polarization layers emit radiation in one phase. Therefore, we can describe the dependence for the forward DR in x-ray range as an interference phenomena between two coherent radiation sources. Note that radiation from the first surface (BC facet) into an electron propagation direction goes through the screen and undergoes an absorption that could be characterized by absorption length. According to classical macroscopic electrodynamics [61], the radiation will be completely absorbed under the condition

$$a \gg l_{\mathrm{abs}} = \frac{\lambda}{4\pi\,\mathrm{Im}\sqrt{\varepsilon}}, \tag{40}$$

where l_{abs} is the absorption length. Thus, when the longitudinal screen dimension becomes greater than l_{abs}, only the forward DR from the second surface (AD facet) can be observed. In Fig. 4 we mark the value of a length equal to $4\pi l_{\mathrm{abs}}$ and claim that the radiation generated by the BC facet is completely absorbed by the screen material at this distance.

Hence, in the case of forward DR the polarization layer thickness, which is the radiation source, can be obtained from Fig. 4 and corresponds to half of the function period or the coherence length.

As is generally known for Cherenkov effect, which could be explained as coherence interaction of all emitted waves, the coherence length extends to infinity [67]. For this reason we do not observe any oscillations for ChR dependence in Fig. 4. The phenomena of saturation must be determined only by the influence of the absorption properties of the medium in the radiation process. Understandably, not all emitted photons manage to leave the screen.

We further note that the above relationships can be obtained in general form from the macroscopic approach if we consider Eq. (25). The simple term, which includes an exponent with a complex argument, describes the dependence of the intensity of emitted photons on longitudinal screen size a. The previously mentioned factor can be presented as a multiplication of two exponents, which depend on real and imaginary parts of the dielectric permittivity. We can rewrite the exponent with a complex argument that depends on the real part of permitivitty using Euler's formula. In this way, the dependence of the radiation intensity on the longitudinal screen size takes the form

$$\left|1 - \exp\left[-ia\frac{\omega}{\beta c}(1 - \beta\,\mathrm{Re}\sqrt{\varepsilon}\cos\theta - i\beta\,\mathrm{Im}\sqrt{\varepsilon}\cos\theta)\right]\right|^2 = e^{-2y}|e^{y} - \cos x - i\sin x|^2, \tag{41}$$

where

$$x = a\frac{\omega}{\beta c}(1 - \beta\,\mathrm{Re}\sqrt{\varepsilon}\cos\theta),$$
$$y = a\frac{\omega}{c}\,\mathrm{Im}\sqrt{\varepsilon}\cos\theta.$$

Let us consider the case for when Eq. (41) provides a maximum radiation intensity. The negligibly small parameter y is the main condition because an increase of the component drives the exponential decrease in the radiation intensity. Hence, the radiation intensity will have a maximum value when component $y = 0$ and Eq. (41) can be significantly simplified:

$$|1 - \cos x - i\sin x|^2 = 2(1 - \cos x). \tag{42}$$

From the relationship in Eq. (42) one can see that radiation intensity has a maximum magnitude when $\cos x = -1$ (i.e., when the radiation is emitted coherently), if the longitudinal screen size satisfies the criteria

$$a_{\mathrm{coh}} = (2n+1)\frac{\pi c}{\omega}\frac{\beta}{|1 - \beta\,\mathrm{Re}\sqrt{\varepsilon}\cos\theta|} = \frac{2n+1}{2}\frac{\lambda}{|\beta^{-1} - \mathrm{Re}\sqrt{\varepsilon}\cos\theta|}. \tag{43}$$

Equation (43) coincides with Eq. (39), which is derived by the microscopic approach. Naturally for the case of the Cherenkov effect, the dependence of the coherent length on the observation angle coincides with the earlier results obtained by Pafomov [67].

In considering the problem of radiation in an absorbing medium, one can claim that its intensity exponentially decreases and that it is characterized by absorption length. The expression for absorption length is obtained from Eq. (41) under the condition $2y = 1$. For this case, the radiation intensity decreases by e times, when the longitudinal screen size corresponds to

$$a_{\mathrm{abs}} = \frac{c}{2\omega\,\mathrm{Im}\sqrt{\varepsilon}\cos\theta} = \frac{\lambda}{4\pi\,\mathrm{Im}\sqrt{\varepsilon}\cos\theta}. \tag{44}$$

Equation (44) derived above coincides with Eq. (40). We must mention that, in general, the absorption length depends on the radiation-spread direction. Therefore, the x-ray ChR absorption is proportional to the relationship between the real and imaginary parts of dielectric permittivity:

$$a_{\mathrm{abs}} \propto \sqrt{\frac{\mathrm{Re}\,\varepsilon}{\mathrm{Im}\,\varepsilon}}.$$

There is yet another factor which can influence the intensity of PR and consequently suppress interference. As an example, Fig. 5 shows the dependencies of the intensity of the emitted photons in the given directions on the transverse screen size d (see Fig. 1) for an electron traveling in the vicinity of an aluminum foil. Figure 5 shows the dependencies corresponding to different respective observation angles $\theta = 0$ and $\theta_c = 15.31^\circ$ for forward DR and ChR. The selected calculation parameters

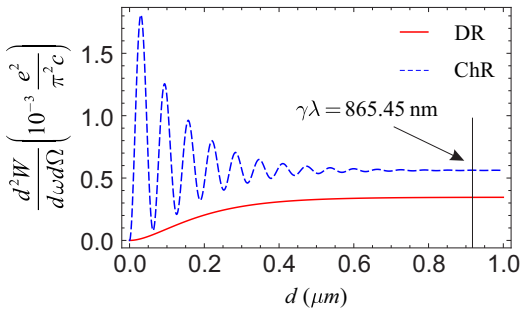

FIG. 5. (Color online) The PR intensity emitted by an electron of energy $\gamma = 50$ at maximum of a spectral-angular distribution in θ as a function of transverse size d of aluminum foil. The red solid and the blue dashed curves correspond to the forward DR ($\theta = 0$) and ChR ($\theta_c = 15.31^\circ$), respectively. Parameters are $a = 0.1$ mm, $b = 1$ μm, $\phi = 0$, and the x-ray energy near absorption of the L edge of aluminum is 72.6 eV.

are as follows: the impact factor is $b = 1$ μm, the longitudinal screen size is $a = 0.1$ mm, and the electron energy is $\gamma = 50$.

According to Ref. [70], the typical transverse radiator size contributing to TR or DR generation is $\gamma\lambda$. As we expected, the intensity of forward DR rises with increasing transverse screen size and then saturates, which can be explained by attenuation of the electromagnetic field of a charge.

For the case of Cherenkov emission, the radiation intensity dependence is also a rapidly oscillating function that decays with increasing transverse screen size. To understand this radiation behavior, we must note that the formation of ChR comes from the polarization current occurring at the interfaces between mediums [44]. For the case of the radiation geometry illustrated in Fig. 1 the screen facets AB and CD are the potential sources of Cherenkov emission in the x-ray range. Therefore, we can obtain the dispersion relationship for oscillation function using the microscopic approach.

Let us consider the scattering of one Fourier component of the self-field of a fast charge from two identical atoms at points $\mathbf{R}_1$ and $\mathbf{R}_2$ on the y axis for a fast charge moving uniformly in vacuum in a direction perpendicular to the y axis. According to the microscopic theory developed in Ref. [39], the spectral-angular radiation distribution created by the Fourier component of the field of the fast charge can be found as

$$\frac{d^2W}{d\omega d\Omega} = \frac{\omega^2}{c}|\alpha(\omega)|^2|[\mathbf{k}\times\mathbf{E}_0(\mathbf{q},\omega)]|^2 \times 2\{1-\cos[(\mathbf{q}-\mathbf{k})\cdot(\mathbf{R}_1-\mathbf{R}_2)]\}, \quad (45)$$

where $\alpha(\omega)$ is the polarizability of the atom, $\mathbf{q} = \frac{\omega}{v}(0,0,1)$ is the wave vector of the transmitted wave, and $\mathbf{k} = \frac{\omega}{c}\sqrt{\varepsilon}(0,\sin\theta,\cos\theta)$ is the wave vector of scattering wave under observation angle θ (refer to Eq. (2.9) in Ref. [39]).

For the case under consideration, vector $\mathbf{R}_1 - \mathbf{R}_2$ is directed along the y axis; hence, $(\mathbf{q}-\mathbf{k})\cdot(\mathbf{R}_1-\mathbf{R}_2) = (q_y - k_y)(Y_1 - Y_2) = L(-k_y)$. Therefore, the factor $2[1+\cos(Lk_y)]$ takes a value from 0 to 4 in accord with the cosine argument $(\mathbf{q}-\mathbf{k})\cdot(\mathbf{R}_1-\mathbf{R}_2) = Lk_y$. For $Lk_y \ll 1$, this factor is equal to 4. For this reason the energy emitted by two atoms is four times higher than the energy emitted by one atom. This means that waves emitted by both atoms are coherent, i.e., arrive at a point of observation with the same phases, and their amplitudes are summed. As a result, the radiation field is doubled and the energy reaching the observation point is quadrupled. If $Lk_y \gg 1$, $\cos(Lk_y)$ is a rapidly oscillating function.

Thus, the condition of the radiation coherence from two atoms can be written in the form

$$L \ll d_{\rm coh}, \quad (46)$$

where the length

$$d_{\rm coh} \sim \frac{\lambda}{\sin\theta\,{\rm Re}\sqrt{\varepsilon}} \quad (47)$$

may be called the coherence depth or the formation depth similarly to coherent length.

However, according to Eq. (45), radiation from two atoms can also be coherent under the condition

$$L = d_{\rm coh}n. \quad (48)$$

Thus, two atoms of the medium will emit coherently if the distance between them is equal to an integer number n of coherence depth $d_{\rm coh}$.

As shown in Fig. 5, the dependence of ChR intensity on the transverse dimension d of an aluminum screen is an oscillation function with a period $d_{\rm coh} = 63.13$ nm. When the transverse dimension of a target becomes greater than the typical transverse radiator size $\sim\gamma\lambda$, only radiation from the first boundary between two mediums (AB facet in Fig. 1) is observable. The computation results also indicate that the polarization layers thickness for Cherenkov emission can be determined as a half of the coherence depth.

Using the macroscopic approach, the expression for coherence depth (47) can be easily derived from Eq. (25) when considering the case for maximum radiation intensity. For this purpose we present a factor that includes the transverse screen size d, in the same way as expression (41),

$$\left|\exp\left\{-id\frac{\omega}{\beta c}[\beta({\rm Re}\sqrt{\varepsilon}+i\,{\rm Im}\sqrt{\varepsilon})\sin\theta\cos\phi - i\gamma^{-1}({\rm Re}\,K + i\,{\rm Im}\,K)]\right\}\right|^2 = e^{-2y}|e^y - \cos x + i\sin x|^2, \quad (49)$$

where

$$x = d\frac{\omega}{\beta c}(\beta\,{\rm Re}\sqrt{\varepsilon}\sin\theta\cos\phi + \gamma^{-1}\,{\rm Im}\,K),$$
$$y = d\frac{\omega}{\beta c}(\gamma^{-1}\,{\rm Re}\,K - \beta\,{\rm Im}\sqrt{\varepsilon}\sin\theta\cos\phi).$$

Consequently, the radiation intensity will decrease by e times under condition $2y = 1$, which corresponds to the transverse screen size:

$$d_{\rm abs} = \frac{\gamma\beta c}{2\omega({\rm Re}\,K - \gamma\beta\,{\rm Im}\sqrt{\varepsilon}\sin\theta\cos\phi)} = \frac{\gamma\beta\lambda}{4\pi({\rm Re}\,K - \gamma\beta\,{\rm Im}\sqrt{\varepsilon}\sin\theta\cos\phi)}. \quad (50)$$

For the case of DR, the coherence depth (47) agrees with the value of the effective attenuation radius of electromagnetic field $\propto \gamma\beta\lambda$.

If we consider Eq. (49) in the same way as for coherence length (43) under the condition $\cos x = -1$, we can get the expression for coherence depth:

$$d_{\mathrm{coh}} = \frac{(2m+1)\pi\beta c}{\omega(\beta\,\mathrm{Re}\,\sqrt{\varepsilon}\sin\theta\cos\phi + \gamma^{-1}\,\mathrm{Im}\,K)} = \frac{2m+1}{2}\frac{\beta\lambda}{\beta\,\mathrm{Re}\,\sqrt{\varepsilon}\sin\theta\cos\phi + \gamma^{-1}\,\mathrm{Im}\,K}. \quad (51)$$

Equation (51) completely agrees with the results (47) obtained by the microscopic approach.

Investigations performed in this section agree well with predictions made by microscopic theory and open up new possibilities for increasing the intensity of x-ray Cherenkov emission from multilayer screens. The examples presented above indicate that radiator dimensions affect the intensity of different types of radiations and can increase the contrast between different radiations.

C. Dependence of PR intensity on a charged particle's energy

As we mentioned briefly in the Introduction, the last experimental and theoretical studies [25–27] showed that the brightness of PR, which can be achieved by passing a low-energy electron beam (a few MeV) through a thin foil, is sufficient for practical x-ray microscopy. Therefore, the critical need is to address the dependence of the Cherenkov emission intensity on electron energy and to compare the intensities of simultaneous radiations (DR or TR).

The considered approach enables us to calculate the spectral-angular distribution of PR for various electron energies and plot the desirable dependencies. Figure 6 shows results for intensities at the maxima of spectral-angular distribution for an electron traveling at a distance $b = 1\ \mu$m from an aluminum foil with fixed sizes. To avoid any effects induced by the coherence length (or depth), the dependencies were obtained only under the condition where the dimensions of the foil were at least several orders of magnitude larger than the coherence length (or depth). We made a similar estimation for different target materials and claim that the obtained dependencies are monotonically increasing functions of electron energy for both types of radiation. For a low-energy electron that reaches the Cherenkov threshold $v > c/\,\mathrm{Re}\,\sqrt{\varepsilon}$, the intensity of the Cherenkov emission is predominant over DR (or TR), but the flux of x-ray photons is ultraweak.

If electron energy increases, the intensity of DR (or TR) will begin to exceed the Cherenkov emission with a dramatically enhanced contrast. Hence, the intricacy determined by an interference effect in the interpretation of the obtained results disappears.

For the ultrarelativistic case, Eq. (25) becomes independent of electron energy. This conclusion agrees fully with well-known results obtained by different approaches for the ultrarelativistic electron energy limit [29,40].

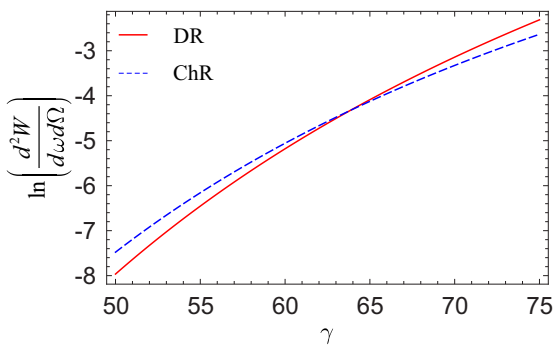

FIG. 6. (Color online) The PR intensity emitted at the maximum of spectral-angular distribution in θ as a function of an electron energy γ. The red solid and the blue dashed curves correspond to the forward DR ($\theta = 0$) and ChR ($\theta_c = 15.31^\circ$), respectively. Parameters are $a = 0.1$ mm, $d = 10$ mm, $b = 1\ \mu$m, $\phi = 0$, and the energy of x ray near the absorption L edge of aluminum is 72.6 eV. Note that the Y axis is logarithmic.

D. Spectrum dispersion of x-ray Cherenkov emission

For an experimental study of Cherenkov x rays, measurements of the photon energy and angular distribution are essential for interpreting experimental data. The photon energy in the x-ray range is typically measured by detecting the photon flux passing through different optical elements [4]. Thus, the spectral resolution of a detector system and the employed optical elements will determine the measured spectrum.

Therefore, the theoretical results obtained for the fixed photon energy are not suitable for estimating the photon yield, as it would require future experimentation. To calculate the photon flux for averaged energy, we propose employing the complex permittivity as a function of photon energy. As shown in a previous section, Henkel's model enables us to derive complex permittivity using the scattering factors.

Figure 7 illustrates the experimental data and approximations curves for the real and imaginary parts of the aluminum scattering factor as a function of photon energy. To describe the real and imaginary parts of aluminum scattering factor we

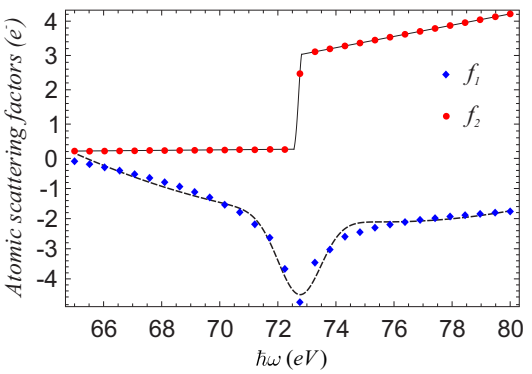

FIG. 7. (Color online) The real and imaginary components of the aluminum scattering factor for x rays as a function of photon energy. The blue diamonds and red circles correspond, respectively, to the real and imaginary parts of the aluminum scattering factor. Similarly, the dashed and solid curves correspond, respectively, to the approximation functions for the real and imaginary parts of scattering factor.

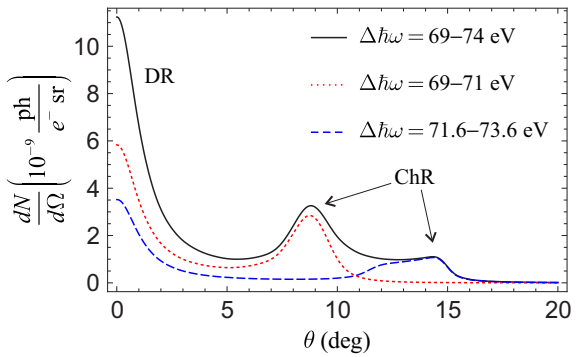

FIG. 8. (Color online) Spectral-angular distribution of PR in θ emitted by an electron of energy $\gamma = 48$ from aluminum foil for the different cases of averaged photon energy. The black solid, the red dotted, and blue dashed curves correspond, respectively, to $\Delta\hbar\omega = 69$–74 eV, $\Delta\hbar\omega = 69$–71 eV, and $\Delta\hbar\omega = 71.6$–73.6 eV, the averaging photon energy. Parameters are $a = 5$ μm, $d = 10$ mm, $b = 1$ μm, and $\phi = 0$.

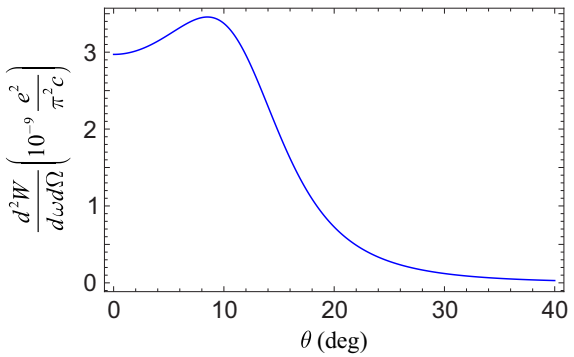

FIG. 9. (Color online) Spectral-angular distribution of PR in θ emitted by an electron of energy $\gamma = 50$ from aluminum foil. Parameters are $a = 0.8$ μm, $d = 8$ nm, $b = 1$ μm, $\phi = 0$, and the x-ray energy is 80 eV.

apply the respective approximation functions,

$$f_1(\hbar\omega) = -2.59\,\exp\left[-\frac{(\hbar\omega - 72.7424)^2}{1.0805}\right] + 111.9440 - 3.0130\,\hbar\omega + 0.0199(\hbar\omega)^2,$$

$$f_2(\hbar\omega) = \begin{cases} -0.2547 + 0.0072\hbar\omega, & \text{I} \\ 3.1687\,\exp\left[-\frac{(\hbar\omega - 72.8539)^2}{0.0356}\right], & \text{II} \\ -8.9201 + 0.1642\hbar\omega, & \text{III} \end{cases}$$

where I, II, and III correspond, respectively, to $\hbar\omega \leqslant 72.55$ eV, 72.55 eV $< \hbar\omega \leqslant 72.82$ eV, and 72.82 eV $< \hbar\omega \leqslant 80$ eV energy ranges.

Angular distributions of x-ray PR illustrated in Fig. 8 are calculated using the presented approximation functions for various average photon energy near the L edge of aluminum. As clearly seen in Fig. 8, aluminum has a very large spectral dispersion and will satisfy the Cherenkov criteria for a broad energy range near the L edge. Thus, the existence of spectral dispersion may pose difficulties in explaining the experimental data. Conversely, the broad spectral dispersion of Cherenkov emission can open new opportunity for many x-ray microscopy applications. For example, the x-ray ChR may be applied as a broadband source in x-ray range with specific angular distributions, which depend on radiation energy. Another active area of research can be the determination of the real part of complex permittivity of different materials from spectral-angular measurements.

For these reasons the question of a photon energy range that satisfies the Cherenkov criteria becomes essential for many applications. To justify our assumption, we intentionally studied the angular distribution of PR from aluminum foil with a selected photon energy, 80 eV, which does not correspond to x-ray energy near any absorption edge of aluminum. To simplify explanation of the obtained result, we used specific screen dimensions in our calculation. For instance, to suppress forward DR, the transverse screen size was configured to be 8 nm. As is shown from Fig. 9 the maximum intensity of the considered distribution corresponds to 8.5°, which satisfies the condition $\cos\theta_c = c/\,\text{Re}\,\sqrt{\varepsilon}v$.

At the end of this section we may conclude that photon energy near the absorption edges is not a requirement for the appearance of Cherenkov x rays. The well-known Cherenkov criteria plays the main role in the x-ray range. However, the yield of Cherenkov rays are great near the absorption edges of mediums compared to other spectral ranges and are determined by two factors. First, the real part of permittivity is sharply enhanced near the absorption edges. Second, the imaginary part of permittivity, which corresponds to the absorption properties of the medium, may be weak. These subtleties are in good agreement with the criteria $\text{Re}\,\varepsilon - 1 > \text{Im}\,\varepsilon$ proposed by Bazylev for x ray Cherenkov emission [18,19].

IV. CONCLUSIONS

In this paper, PCA has been applied to study in detail the x-ray radiation emitted by a charged particle traveling in the vicinity of an absorbing foil. We demonstrated that x-ray Cherenkov emission could be considered as a radiation of polarization currents induced in the bulk of a medium by the Coulomb field of a charged particle. PCA enables us to obtain well-known results from existing theories and account for the absorption properties of the medium and the real shape of a target. Using simplified radiation geometry, we demonstrated how to derive all features of emitted radiation including the polarization properties for a wide energy range of a charged particle. The influence of finite foil sizes, which can effectively increase the yield of Cherenkov x rays, was studied by both macroscopic and microscopic electrodynamics methods. It was found that the Cherenkov effect in the x-ray range might occur even beyond the near vicinity of the absorption atomic edges of a medium. The Cherenkov criteria is still the main condition for radiation emergence in the x-ray range, and the relation $\text{Re}\,\varepsilon - 1 > \text{Im}\,\varepsilon$ proposed by Bazylev is required to observe the x-ray Cherenkov effect in real experimental studies.

We would like to emphasize that the obtained results can potentially lead to a high level of understanding of the features of emitted radiation and enable us to develop new sources of radiation in the soft x-ray range based on the Cherenkov effect.

ACKNOWLEDGMENTS

The authors acknowledge fruitful discussions with Professor A. Potylitsyn and Dr. S. Uglov. This work was partly supported by Photon and Quantum Basic Research Coordinated Development Program from the Ministry of Education, Culture, Sports, Science and Technology, Japan, the program "Nauka" of the Russian Ministry of Education and Science within the Grant No. 3.709.2014/K and the Competitiveness Enhancement Program of Tomsk Polytechnic University. We would also like to acknowledge the Russian Foundation for Basic Research (Grants No. 14-02-31642-mol_a, No. 14-02-01032-A, and No. 15-52-50028 YaF_a).

[1] W. Chao *et al.*, Nature (London) **435**, 1210 (2005).
[2] M. M. Barysheva *et al.*, Phys.-Usp. **55**, 681 (2012).
[3] D. Attwood, *Soft X-rays and Extreme Ultraviolet Radiation. Principles and Applications* (Cambridge University Press, Cambridge, U.K., 1999).
[4] A. Sakdinawat and D. Attwood, Nat. Photon. **4**, 840 (2010).
[5] T. Kimura *et al.*, Nat. Commun. **5**, 3052 (2014).
[6] S. Stuchebrov *et al.*, J. Phys.: Conf. Ser. **517**, 012046 (2014).
[7] S. Stuchebrov *et al.*, Adv. Mater. Res. **880**, 168 (2014).
[8] B. L. Henke, E. M. Gullikson, and J. C. Davis, At. Data Nucl. Data Tables **54**, 181 (1993).
[9] Ph. Zeitoun *et al.*, Nature (London) **431**, 426 (2004).
[10] T. Popmintchev *et al.*, Proc. Natl. Acad. Sci. USA **106**, 10516 (2009).
[11] P. W. Wachulak *et al.*, Nucl. Instrum. Methods Phys. Res., Sec B **268**, 1692 (2010).
[12] H. Legall *et al.*, Opt. Express **20**, 18362 (2012).
[13] I. Frank and Ig. Tamm, C. R. Acad. Sci. USSR **14**, 109 (1937).
[14] G. N. Afanasiev, *Vavilov-Cherenkov and Synchrotron Radiation. Foundations and Applications* (Springer, Berlin, 2005).
[15] O. V. Bogdanov, E. I. Fiks, and Yu. L. Pivovarov, J. Exp. Theor. Phys. **115**, 392 (2012).
[16] M. A. Piestrup, R. H. Pantell, H. E. Puthoff, and G. B. Rothbart, J. Appl. Phys. **44**, 5160 (1973).
[17] M. A. Piestrup *et al.*, Appl. Phys. Lett. **28**, 92 (1976).
[18] V. A. Bazylev *et al.*, JETP Lett. **24**, 371 (1976).
[19] V. A. Bazylev *et al.*, Sov. Phys. JETP **54**, 884 (1981).
[20] M. J. Moran, B. Chang, and M. B. Schneider, Nucl. Instrum. Methods Phys. Res., Sec. B **48**, 287 (1990).
[21] C. Gary *et al.*, Nucl. Instrum. Methods Phys. Res., Sec. B **227**, 95 (2005).
[22] A. Kubankin *et al.*, Radiat. Phys. Chem. **75**, 913 (2006).
[23] J. M. Corstens and M. J. van der Wiel, Nucl. Instrum. Methods Phys. Res., Sec. B **262**, 368 (2007).
[24] W. Knulst, Ph.D. thesis, Thechnische Universität Eindhoven, 2004.
[25] A. E. Kaplan and P. L. Shkolnikov, Appl. Phys. Lett. **86**, 024107 (2005).
[26] W. Knulst, O. J. van der Wiel, and J. Verhoeven, Appl. Phys. Lett. **79**, 2999 (2001).
[27] W. Kunlst *et al.*, Appl. Phys. Lett. **83**, 4050 (2003).
[28] V. L. Ginzburg and I. M. Frank, Sov. Phys. JETP **16**, 15 (1946) [in Russian].
[29] V. L. Ginzburg and V. N. Tsytovich, *Transition Radiation and Transition Scattering* (Hilger, Bristol, New York, 1990).
[30] D. V. Karlovets and A. P. Potylitsyn, JETP Lett. **90**, 326 (2009).
[31] D. V. Karlovets, J. Exp. Theor. Phys. **113**, 27 (2011).
[32] V. P. Zrelov and J. Ružička, Nucl. Instrum. Methods **160**, 327 (1979).
[33] V. L. Ginzburg and I. M. Frank, Dokl. Akad. Nauk SSSR **56**, 699 (1947) [in Russian].
[34] M. B. Bolotovskii, Sov. Phys. Usp. **4**, 781 (1962).
[35] G. A. Naumenko, A. P. Potylitsyn, M. V. Shevelev, and Y. A. Popov, JETP Lett. **94**, 258 (2011).
[36] S. N. Galyamin and A. V. Tyukhtin, Phys. Rev. Lett. **113**, 064802 (2014).
[37] E. S. Belonogaya, S. N. Galyamin, and A. V. Tyukhtin, J. Opt. Soc. Am. B **32**, 649 (2015).
[38] A. A. Tishchenko, A. P. Potylitsyn, and M. N. Strikhanov, Phys. Lett. A **359**, 509 (2006).
[39] A. P. Potylitsyn, M. I. Ryazanov, M. N. Strikhanov, and A. A. Tishchenko, *Diffraction Radiation from Relativistic Particles*, Springer Tracts in Modern Physics Vol. 239 (Springer, Berlin, 2010).
[40] A. P. Potylitsyn, Nucl. Instrum. Methods Phys. Res., Sect. B **145**, 169 (1998).
[41] M. I. Ryazanov and I. S. Tilinin, Sov. Phys. JETP **44**, 1092 (1976).
[42] M. Ya. Amusia, Radiat. Phys. Chem. **75**, 1232 (2006).
[43] K. O. Kruchinin and D. V. Karlovets, Russ. Phys. J. **55**, 9 (2012).
[44] M. V. Shevelev and A. S. Konkov, J. Exp. Theor. Phys. **118**, 501 (2014).
[45] G. Naumenko *et al.*, J. Phys.: Conf. Ser. **517**, 012004 (2014).
[46] V. V. Bleko, A. S. Konkov, and V. V. Soboleva, Nucl. Instrum. Methods Phys. Res., Sect. B **355**, 129 (2015).
[47] I. P. Ivanov and D. V. Karlovets, Phys. Rev. Lett. **110**, 264801 (2013).
[48] I. P. Ivanov and D. V. Karlovets, Phys. Rev. A **88**, 043840 (2013).
[49] J. D. Jackson, *Classical Electrodynamics* (Wiley & Sons, New York, London, 1962).
[50] R. W. James, *The Optical Principles of the Diffraction of X Rays* (Bell & Sons, London, 1948).
[51] A. E. Kaplan, C. T. Law, and P. L. Shkolnikov, Phys. Rev. E **52**, 6795 (1995).
[52] B. L. Henke *et al.*, At. Data Nucl. Data Tables **27**, 1 (1982).
[53] Rod Vance, *Discussions about complex emissivity and complex permeability*, http://physics.stackexchange.com/questions/81950/question-about-complex-emissivityand-complex-permeability.
[54] R. P. Feynman, R. B. Leighton, and M. Sands, *The Feynman Lectures on Physics: Mainly Electromagnetism and Matter* (Addison-Wesley, London, 1964), Vol. 2.
[55] L. D. Landau and E. M. Lifshits, *Course of Theoretical Physics: Electrodynamics of continuous media* (Butterworth-Heinemann, Oxford, 2004), Vol. 8.

[56] V. M. Agranovich and Yu. N. Gartstein, Usp. Fiz. Nauk **49**, 1029 (2006).
[57] G. V. Rozenberg, Usp. Fiz. Nauk **56**, 77 (1955) [in Russian].
[58] A. P. Potylitsyn, *Electromagnetic Radiation of Electrons in Periodic Structures*, Springer Tracts in Modern Physics Vol. 243 (Springer, Berlin, 2011).
[59] W. A. Shurkliff, *Polarized Light: Production and Use* (Harvard University Press, Cambridge, MA, 1962).
[60] L. D. Landau and E. M. Lifshits, *Course of Theoretical Physics: The Classical Theory of Fields* (Butterworth-Heinemann, Oxford, 1980), Vol. 2.
[61] M. Born and E. Wolf, *Principles of Optics*, 4th ed. (Pergamon Press, London, 1970).
[62] M. I. Ryazanov, JETP Lett. **39**, 698 (1984).
[63] G. S. Ohm, *Die galvanische Kette, mathematisch bearbeitet* (T. H. Riemann, Berlin, 1827) [in German].
[64] E. D. Purcell, *Electricity and Magnetism*, 2nd ed., Berkeley Physics Course Vol. 2 (Cambridge University Press, Cambridge, 1984).
[65] A. Sommerfeld, *Electrodynamics*, Lectures on Theoretical Physics Vol. III (Academic Press, New York, 1952).
[66] A. Ts. Amatuni and N. A. Korkhmazyan, Sov. Phys. JETP **12**, 703 (1961).
[67] V. E. Pafomov, Trudy FIAN **44**, 28 (1969) [in Russian].
[68] A. I. Alekseev and V. V. Yakimets, Sov. Phys. JETP **24**, 1057 (1967).
[69] K. A. Ispirian, in *Advanced Radiation Sources and Applications*, edited by H. Wiedeman (Springer, Netherlands, 2006), p. 217.
[70] N. F. Shul'ga and S. N. Dobrovol'skiĭ, JETP Lett. **65**, 614 (1997).